ISSN (Print) 1226-1750
ISSN (Online) 2233-6656
Journal of Magnetics 19(3), 221-226 (2014) http://dx.doi.org/10.4283/JMAG.2014.19.3.221

Magneto-transport Properties of $La_{0.7}Sr_{0.3}Mn_{1+d}O_3$-Manganese Oxide Composites Prepared by Liquid Phase Sintering

Hyo-Jin Kim[1], Jae-Hyoung You[1], Soon-Mi Choi[1], and Sang-Im Yoo[1]*

[1]*Department of Materials Science and Engineering, Research Institute of Advanced Materials (RIAM), Seoul National University, Seoul 151-744, Korea*

(Received 23 June 2014, Received in final form 14 August 2014, Accepted 19 August 2014)

Significantly enhanced low-field magnetoresistance (LFMR) and maximum dMR/dH {(dMR/dH)$_{max}$} values were successfully achieved from $La_{0.7}Sr_{0.3}MnO_3$(LSMO)-manganese oxide composite samples prepared by liquid phase sintering, compared with those of the same composites prepared by solid state reaction. For this study, pure LSMO and LSMO-manganese oxide composites with various nominal compositions of (1-x)LSMO–$x$$Mn_2O_3$ (x = 0.1, 0.2, 0.3, 0.4, and 0.8) were sintered at 1450°C, above the eutectic temperature of 1430°C, for 1 h in air. The highest LFMR value of 1.28% with the highest (dMR/dH)$_{max}$ value of 21.1% kOe^{-1} was obtained from the composite sample with x = 0.3 at 290 K in 500 Oe. This enhancement of LFMR and (dMR/dH)$_{max}$ values is ascribed to efficient suppression of magnetic disorder at the LSMO grain boundary, by forming a characteristic LSMO-manganese eutectic structure.

Keywords : perovskite manganite, LFMR (low field magnetoresistance), magnetotransport property

1. Introduction

$RE_{1-x}A_xMnO_3$ perovskite manganites (where RE is a rare earth element, and A is a divalent cation), commonly exhibiting the colossal magnetoresistance effect, have been studied worldwidely because of their abundant physical properties and potential applications, such as magneto-resistive transducers and sensors [1, 2]. These perovskite maganites are also known to exhibit the LFMR effect in the form of polycrystalline samples, but not in the form of epitaxial thin films or single crystals [3]. Among these manganites, LSMO shows the highest Curie temperature ($T_C \approx$ 360 K), which makes it possible to fabricate a device that operates at room temperature. The LFMR effect, normally observed at the temperatures below T_C in low fields (< 0.2 T), is attributable to a spin-polarized tunneling of the transport electrons at the grain boundaries [3, 4]. Thus, it is very important to control the microstructures of LSMO polycrystalline samples for the enhancement of the LFMR effect.

Since the LFMR values of pure $RE_{1-x}A_xMnO_3$ perovskite maganites are insufficient for real applications, many groups have attempted to improve the LFMR effect by producing composites of manganites with second phases, such as insulating oxides [5-13], metals [14, 15], polymers [16, 17], and other manganites [18-20]. In comparison with a pure polycrystalline manganite, the perovskite manganite-oxide composites exhibited much improved LFMR effect, which was normally accompanied by a significant increase in their electrical resistivities and an abrupt decrease in their T_C values. We have recently reported that the second phases, like Mn_2O_3 (or Mn_3O_4) [22] and La_2O_3 [23], chemically compatible with LSMO [21], were very effective for avoiding such serious degradation in both T_C and electrical conductivity. As a new approach to improve the LFMR effect of LSMO, we tried in this study to modify the LSMO grain boundaries by forming the eutectic structure between LSMO and manganese oxide, via liquid phase sintering at a temperature above the eutectic temperature in air of 1430°C [21].

2. Experimental

The precursor materials of La_2O_3, $SrCO_3$, and Mn_2O_3 powders, all with 99.9% purity, were weighed to have the nominal compositions of (1-x) LSMO–$x$$Mn_2O_3$ (x = 0, 0.1, 0.2, 0.3, 0.4, and 0.8), and ball-milled in ethyl alcohol, using ZrO_2 balls for 24 h. The ball-milled slurry was

*Corresponding author: Tel: +82-2-880-5720
Fax: +82-2-887-6388, e-mail: siyoo@snu.ac.kr

dried and calcined twice at 1100°C for 8 h in air. As-calcined powder was uniaxially pressed into pellets with the diameter of 10 mm, and then consolidated by cold isostatic pressing (~2 ton cm^{-2}). The pellets were sintered at 1450°C for 1 h in air. Referring to the La_2O_3-Mn_2O_3 phase diagram [21], we selected 1450°C for liquid phase sintering since the eutectic temperature in air between LSMO and Mn_3O_4 is reported to be 1430°C. In addition, according to the La_2O_3-Mn_2O_3 phase diagram [21] at 1450°C in air, while the sample with the nominal composition of $x = 0$ is pure LSMO phase, LSMO and liquid phase are equilibrium phases for the samples with the nominal compositions of $x = 0.1$-0.4, and Mn_3O_4 and liquid phase are equilibrium phases for the sample with that of $x = 0.8$. Therefore, at 1450°C in air, while LSMO is expected to be sintered by solid state reaction, all composite samples are expected to be densified by liquid phase sintering. Further, the eutectic structures are expected to form from liquid phases, during furnace cooling to room temperature.

Powder X-ray diffraction (XRD, BRUKER D8 ADVANCE) using Cu-$K\alpha$ radiation ($\lambda = 1.54$ Å), and scanning electron microscopy (SEM, JEOL JSM-6360) were performed for the analyses of phases and microstructures, respectively. For the SEM observations, all composite samples were polished, and then thermally etched at 1300°C for 1 h in air. The microstructures were also analyzed by transmission electron microscopy (TEM) (JEOL JEM-3000F, JEM-2100F). The temperature depedency of magnetization (M) was measured with a superconducting quantum interference device (SQUID) magnetometer (MPMS XL5, Quantum Design). The M-T curves were measured with a field-cooled warming procedure, under an applied field of 100 Oe. The Curie temperatures of samples were determined by the maximum $|dM/dT|$ point of the M-T curves. Measurements of LFMR were performed using the standard four-probe method, within the SQUID magnetometer.

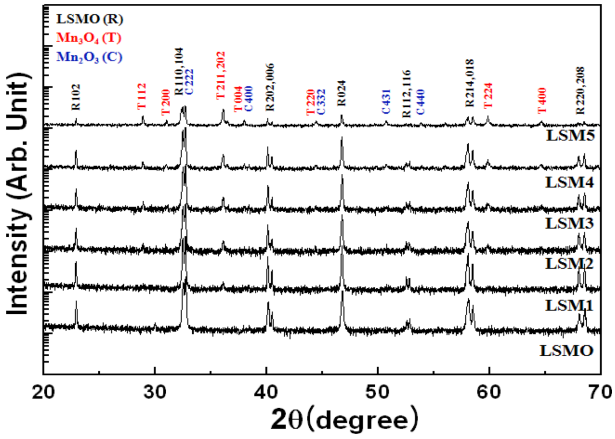

Fig. 1. (Color online) XRD patterns of pure LSMO and LSMO-manganese oxide composites sintered at 1450˚C for 1 h in air.

3. Results and Discussion

Figure 1 shows the powder XRD patterns of pure LSMO and composite samples with the nominal compositions of (1-x) LSMO–x Mn_2O_3 (x = 0.1, 0.2, 0.3, 0.4, and 0.8). Table 1 defines the sample IDs for various nominal compositions. As shown in Fig. 1, the relative peak intensity of tetragonal (T)-Mn_3O_4 gradually increases with increasing Mn_2O_3 mole fraction. According to the La_2O_3-Mn_2O_3 binary phase diagram [21], manganese oxide shows three different phases; cubic (C)-Mn_2O_3 transforms to T-Mn_3O_4 at 880°C and then transforms to C-Mn_3O_4 at 1160°C in air. However, the LSM4 and LSM5 samples, where T-Mn_3O_4 is the major phase, show small peaks of the C-Mn_2O_3 phase, while composite samples, except LSM4 and LSM5, commonly exhibit the T-Mn_3O_4 phase. Similar results were observed in the $La_{0.7}Sr_{0.3}Mn_{1+d}O_3$-manganese oxide composites with the same nominal compositions, prepared by solid state reaction in our previous study [22].

Figure 2 shows SEM micrographs of pure LSMO and

Table 1. Sample identifications (IDs) and properties of the LSMO and LSMO-manganese oxide composite samples. Mn mole fraction, f_{Mn} = Mn/(La+Sr+Mn) in the total precursor powders, sample resistivity (ρ) at 290 K, MR at 290 K in 500 Oe, and maximum MR change (dMR/dH) at 290 K.

Property	Sample IDs					
	LSMO	LSM1	LSM2	LSM3	LSM4	LSM5
f_{Mn}	0.5 ($x = 0$)	0.55 ($x = 0.1$)	0.6 ($x = 0.2$)	0.65 ($x = 0.3$)	0.7 ($x = 0.4$)	0.9 ($x = 0.8$)
ρ (Ωcm)	0.084	0.010	0.041	0.071	0.075	25.834
T_c (K)	368.4	359.4	368.4	365.6	360.2	364.4
MR (%)	1.07	1.06	1.06	1.28	1.27	1.30
dMR/dH (% kOe^{-1})	7.1	8.3	9.2	21.1	25.4	27.8

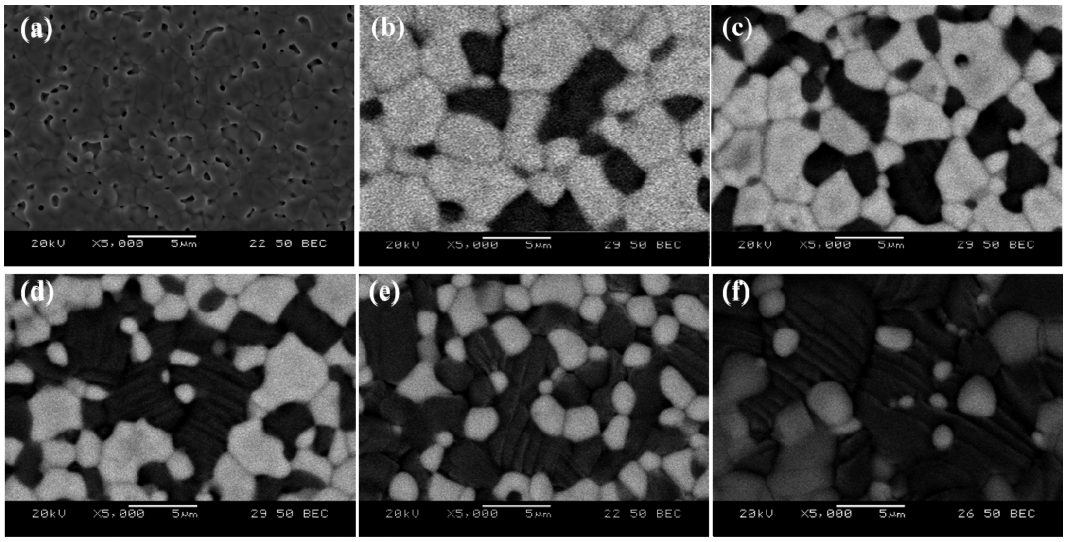

Fig. 2. SEM back-scattered electron images of (a) LSMO, (b) LSM1, (c) LSM2, (d) LSM3, (e) LSM4, and (f) LSM5.

composite samples. While the micrograph in Fig. 2(a) is the surface image of as-sintered LSMO sample, the micrographs in Figs. 2(b)-(f) are the images of thermally etched surfaces of composite samples. Referring to the XRD data, the grains of bright and dark contrast regions for composite samples can be designated as the LSMO and manganese oxide phases, respectively. The average grain size of LSMO decreasing with increasing the amount of manganese oxide can also be seen in the composite samples. These microstructures seem to be somewhat similar to those of our previous study on the same composites prepared by solid state sintering [22], in that the dark contrast region increases with increasing the amount of manganese oxide. However, we can see that the detailed microstructures in Fig. 2 are quite different from those in Ref. [22]. First, compared with pure LSMO sample sintered at 1300°C for 8 h in air in Ref. [22], the pure LSMO sample sintered at 1450°C for 1 h in air in Fig. 2 (a) shows much higher porosity, which is attributed to the overfiring effect at too high a sintering temperature. Next, unlike the typical microstructures of composite samples by the solid state sintering in Ref. [22], all composite samples in Figs. 2(b)-(f) show characteristic microstructures formed by liquid phase sintering. Figures 2(b)-(f) show two different types of LSMO grains of bright contrast; one is relatively large faceted grains connected to each other, and the other is relatively small round-shaped grains surrounded by a dark contrast phase region. On the other hand, Fig. 2(f) shows relatively large faceted Mn_3O_4 grains of less dark contrast, and relatively small round-shaped LSMO grains. In all composite samples, irregular shaped dark contrast regions are composed of many striped Mn_3O_4 grains. Therefore, we suggest that the striped Mn_3O_4 grains and round-shaped LSMO grains might solidify

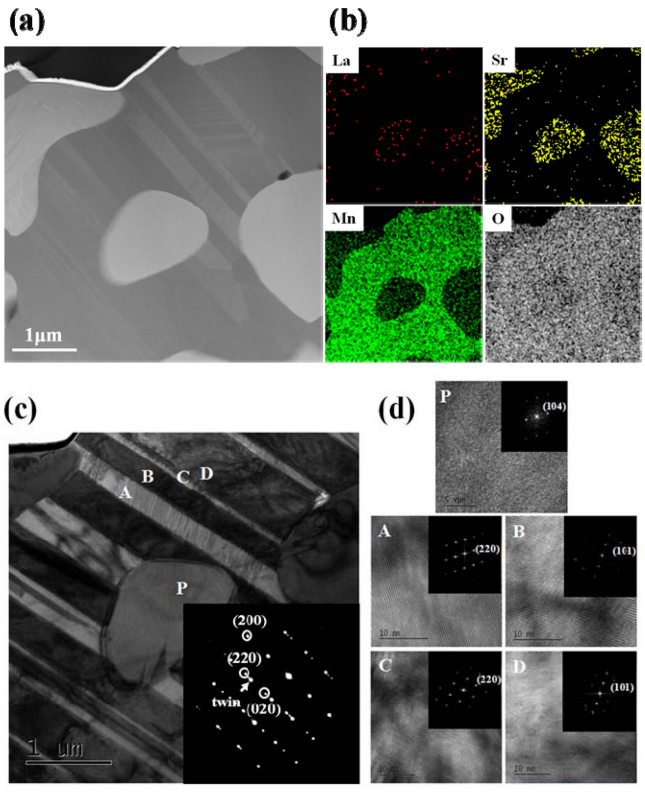

Fig. 3. (Color online) (a) Z-contrast STEM image of the LSM3 sample, and (b) the La, Sr, Mn, and O spectral images. (c) Cross-sectional TEM images of the LSM3 sample. Inset is SAD patterns of A and B areas (d) HR-TEM images of the LSMO (marked by P) and Mn_3O_4 phases (marked by A, B, C, and D). Insets are FFT patterns of A, B, C, and D areas in (c).

from the eutectic liquid phase during furnace-cooling to room temperature, while faceted LSMO and Mn_3O_4 grains were the proeutectic solid phases grown during liquid phase sintering.

To further analyze the microstructure of the composite sample, we performed TEM analyses on the LSM3 sample, as shown in Fig. 3. To identify the LSMO and Mn_3O_4 phases, we also performed the elemental mapping image analysis by scanning transmission electron microscope-energy dispersive spectrometry, as shown in Figs. 3(a) and (b). These data clearly display the LSMO and Mn_3O_4 phase regions. Figure 3(c) shows the bright-field TEM image of the LSM3 sample, where a small LSMO phase surrounded by the Mn_3O_4 phase is shown, representing that both phases were solidified during furnace-cooling. The inset of Fig. 3(c) shows selected area diffraction (SAD) patterns of A and B areas, indicating that the Mn_3O_4 phase from eutectic liquid was grown with twin symmetry. To further analyze the LSMO and Mn_3O_4 phases, HR-TEM analyses were carried out, as shown in Fig. 3(d). The areas of A and C (or B and D) are confirmed to have the same orientation by FFT patterns, supporting the twin relationship in Fig. 3(c).

Figure 4 shows the resistivity curves of all samples. Although the average grain size of LSMO significantly decreases with increasing amount of insulating manganese oxide (Fig. 2), the LSM1, LSM2, LSM3, and LSM4 samples still have lower resistivity than the pure LSMO sample, implying that the LSMO phase of composite samples possesses much lower resistivity value, compared with pure LSMO. Referring to the phase diagram reported by van Roosmalen *et al.* [21], we suggest that the formation of a Mn-excessive LSMO solid solution due to the coexisting manganese oxide in composite samples is mainly responsible for much lowered resistivity in composite samples. Thus, with a small addition of manganese oxide, the resistivity value largely drops (see LSM1 in Fig. 4), and then it gradually increases with further increasing the amount of manganese oxide up to LSM4, in Fig. 4. Resistivity variation similar to this behavior has also been observed for composite samples prepared by solid state sintering in our previous work [22]. In both cases, compared with undoped LSMO, the composite samples may have better inter-granular connectivity, leading to somewhat lower resistivity values. However, since it is impossible to explain such a large decrease in resistivity for the composite samples only with improved inter-granular connectivity between LSMO grains, we suggest the primary reason for this resistivity variation is that Mn-excessive LSMO solid solution grains in the composite samples may have much lower resistivity values, compared with undoped LSMO grains. Interestingly, although conductive LSMO grains seem to be disconnected by insulating manganese oxide grain in Fig. 2(e), this sample shows lower resistivity than the pure LSMO sample. The reason is as follows: The LSMO phase grown from the eutectic liquid phase is believed to not be a round particle but an elongated rod. These rods are connected to each other, and also make bridges between faceted proeutectic LSMO grains. On the other hand, the LSM5 sample shows an abrupt increase in resistivity, since the conducting path of the LSMO phase is seriously blocked by the manganese oxide phase.

Fig. 5 shows the temperature dependency of magnetization for all samples. The T_C values of the composite samples (359-368 K) change insignificantly. These results are quite different from other perovskite manganite-oxide composites [5, 6, 10-13, 18] that show significantly depressed T_C values. The ferromagnetic ordering of LSMO

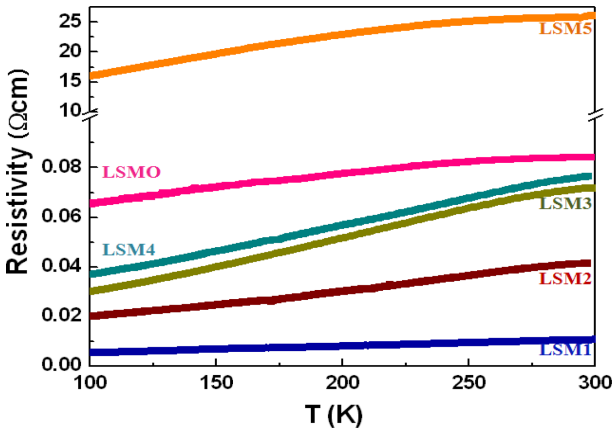

Fig. 4. (Color online) The ρ–T curves for LSMO and LSMO-manganese oxide composite samples.

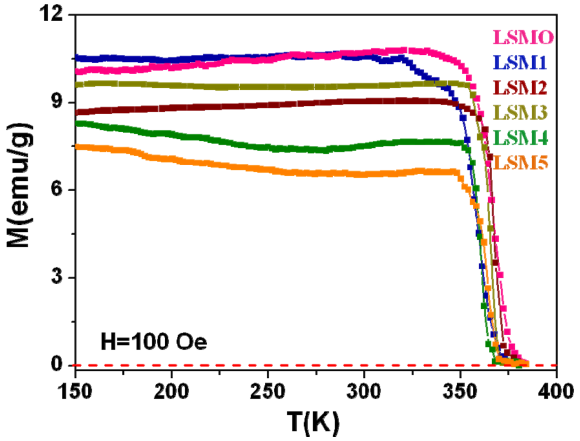

Fig. 5. (Color online) Temperature dependence of magnetization for samples. The M-T curves were measured with field-cooled warming procedure, under an applied field of 100 Oe.

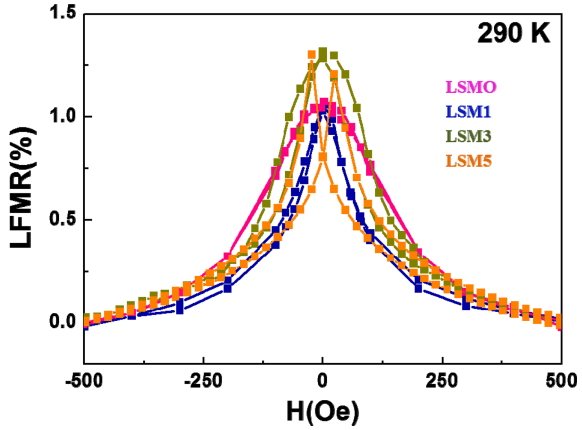

Fig. 6. (Color online) LFMR behaviors of the LSMO and composite samples measured at 290 K in 500 Oe.

is usually weakened by the addition of a secondary phase because of its chemical reaction with LSMO resulting in magnetic dilution [13]. Like our previous results [22, 23], however, the ferromagnetic ordering of the LSMO phase is insignificantly affected by the addition of manganese oxide since LSMO is chemically compatible with manganese oxide.

Fig. 6 represents the LFMR behaviors of samples. We evaluated the LFMR value using the equations of MR (%) = $(R_H - R_{H=500Oe})/R_{H=500Oe} \times 100\%$. Table 1 summarizes the properties of all samples. In comparison with our previous data [22] for the LSMO and LSMO-manganese oxide composite samples prepared by solid state reaction, all composite samples prepared by liquid phase sintering show improved LFMR values. While the LFMR values are unaltered from $x = 0$ to 0.2, those are abruptly increased to ~1.30% from $x = 0.3$ to 0.8, with the same abrupt increase in the $(d\mathrm{MR}/dH)_{max}$ values as listed in Table I. In comparison with pure LSMO, the composite samples surely have higher grain boundary areal density, because of reduction in average grain size (see Fig. 2), and narrower disordered region near the LSMO grain boundary, due to the existence of manganese oxide, which is chemically compatible with LSMO. Therefore, high grain boundary areal density and sharpening of a disordered region near the LSMO grain boundary are believed to be responsible for the enhanced LFMR values of the composite samples. We attribute further improved LFMR properties of these composite samples to an increase in the effective spin scattering center at the grain boundaries.

4. Conclusion

LSMO-manganese oxide composites prepared by liquid phase sintering at 1450°C for 1 h in air turned out to have excellent LFMR effects at room temperature, compared with those of the same composites prepared by solid state reaction. The maximum LFMR value of 1.28%, with $(d\mathrm{MR}/dH)_{max}$ value of 21.1%/kOe at 290 K in 500 Oe, could be achieved from the composite sample of 30 mol% Mn_2O_3 addition. We attribute these results to sharpening of the disordered LSMO grain boundary region acting as more effective spin-dependent scattering centers, by forming the characteristic LSMO-manganese eutectic structure.

Acknowledgement

This work was supported by a Korea Science and Engineering Foundation (KOSEF) grant (No. KRF-0417-20100021), funded by the Korea government (MEST).

References

[1] R. von Helmolt, J. Wecker, B. Holzapfel, L. Schultz, and K. Samwer, Phys. Rev. Lett. **71**, 2331 (1993).
[2] S. Jin, T. H. Tiefel, M. McCormack, R. A. Fastnacht, R. Ramesh, and L. H. Chen, Science **264**, 413 (1994).
[3] H. Y. Hwang, S. W. Cheong, N. P. Ong, and B. Batlogg, Phys. Rev. Lett. **77**, 2041 (1996).
[4] Ll. Balcells, J. Fontcuberta, B. Martínez, and X. Obradors, J. Phys.: Condens. Matter. **10**, 1883 (1997).
[5] A. Gaur and G. D. Varma, J. Alloys Compd. **453**, 423 (2008).
[6] D. K. Petrov, L. Krusin-Elbaum, J. Z. Sun, C. Feild, and P. R. Duncombe, Appl. Phys. Lett. **75**, 995 (1999).
[7] O. A. Shlyakhtin, K. H. Shin, and Y.-J. Oh, J. Appl. Phys. **91**, 7403 (2002).
[8] A. Gaur and G. D. Varma, Cryst. Res. Technol. **42**, 164 (2007).
[9] L1. Balcells, A. E. Carrillo, B. Martínez, and J. Fontcuberta, Appl. Phys. Lett. **74**, 4014 (1999).
[10] A. Gaur and G. D. Varma, Solid State Commun. **139**, 310 (2006).
[11] V. Moshinyaga, B. Damaschke, O. Shapoval, A. Belenchuk, J. Faupel, O. I. Lebedv, J. Verbeeck, G. van Tendeloo, M. Mucksch, V. Tsurkan, R. Tidecks, and K. Samwer, Nat. Mater. **2**, 247 (2003).
[12] C.-H. Yan, Z.-G. Xu, T. Zhu, Z.-M. Wang, F.-X. Cheng, T.-H. Huang, and C.-S. Liao, J. Appl. Phys. **87**, 5588 (2000).
[13] S. Karmakar, S. Taran, B. K. Chaudhuri, H. Sakata, C. P. Sun, C. L. Huang, and H. D. Yang, J. Phys. D: Appl. Phys. **38**, 3757 (2005).
[14] C. Xionga, H. Hu, Y. Xiong, Z. Zhang, H. Pi, X. Wu, L. Li, F. Wei, and C. Zheng, J. Alloys Compd. **479**, 357 (2009).
[15] P. T. Phonga, N. V. Khiem, N. V. Dai, D. H. Manh, L. V. Hong, and N. X. Phuc, J. Alloys Compd. **484**, 12 (2009).

[16] Y.-H. Huang, X. Chen, Z.-M. Wang, C.-S. Liao, and C.-H. Yan, J. Appl. Phys. **91**, 7733 (2002).
[17] J. Kumar, R. K. Singh, H. K. Singh, P. K. Siwach, R. Singh, and O. N. Srivastava, J. Alloys Compd. **455**, 289 (2008).
[18] P. Kameli, H. Salamati, and M. Hakimi, J. Alloys Compd. **463**, 18 (2008).
[19] J.-M. Liu, G. L. Yuan, H. Sang, Z. C. Wu, X. Y. Chen, Z. G. Liu, Y. W. Du, Q. Huang, and C. K. Ong, Appl. Phys. Lett. **78**, 1110 (2001).
[20] C.-H. Yan, F. Luo, Y.-H. Huang, X.-H. Li, Z.-M. Wang, and C.-S. Liao, J. Appl. Phys. **91**, 7406 (2002).
[21] J. A. M. van Roosmalen, P. van Vlaanderen, and E. H. P. Cordfunke, J. Solid State Chem. **114**, 516 (1995).
[22] Y.-M. Kang, H.-J. Kim, and S.-I. Yoo, Appl. Phys. Lett. **95**, 052510 (2009).
[23] H.-J. Kim and S.-I. Yoo, J. Alloys Compd. **521**, 30 (2012).